Impact of the Yoke Material on the Performance of Wounded Electrodynamic Bearings

Corentin Dumont, Virginie Kluyskens, Bruno Dehez

Center for Research in Energy and Mechatronics (CEREM), Université catholique de Louvain (UCL), Place du Levant 2, 1348 Louvain-la-Neuve, Belgium, bruno.dehez@uclouvain.be

***Abstract*—This paper concerns null-flux, centering electrodynamic bearings with an internal rotor made of permanent magnets creating a multipole radial magnetic field and with an external airgap wounded conductor attached to a yoke. The inclusion of a ferromagnetic yoke in front of the permanent magnets has the two following effects. On the one hand, it increases the magnetic flux density in the airgap and the magnitude of the centering Lorentz forces between the rotor and the stator of the device. This is positive since the stiffness associated with the centering force of the bearing increases too. On the other hand, it also induces a negative stiffness due to the reluctant force between the yoke and the magnets usually referred to as the unbalanced magnetic force. The goal of this paper is to investigate about the gain in stiffness and performance associated with the presence of a ferromagnetic yoke in multipole electrodynamic bearings. To this purpose, a method is exposed to evaluate the stiffness and stability of the bearing objectively using a root-loci plot. The results are based on a 2-D analytical model of electrodynamic bearings which is briefly presented in the paper. It is shown that in some cases, the magnetic permeability of the yoke has a very low impact on the bearing performance.**

I. Introduction

Magnetic bearings ensure a contactless guiding function. This makes them more suitable than mechanical bearings for high-speed and/or lubrication-free applications, among others [1]. Nowadays, the magnetic bearings used in the industry are controlled actively. This requires the use of sensors, controllers and power electronics. However, the complexity, cost or bulk associated with this control system can become prohibitive, especially for small rated power applications [2].

A way to overcome these disadvantages could be to use magnetic bearings which do not require external control means i.e., passive bearings. They include supraconducting and electrodynamic bearings. Unlike supraconducting bearings, electrodynamic bearings can operate at room temperature and therefore, they do not require a bulky cooling system. This makes them more compact and simpler [3] and more attractive for stationary applications. Some well-known examples of electrodynamic bearings were studied in [4], [5], [6].

In [7], an analytical study of a new centering electrodynamic bearing with a radial magnetic field was presented. The proposed topology is shown in Fig. 1. It has an internal rotor comprising a ferromagnetic shaft and permanent magnets generating a multipole radial magnetic field in the airgap. The stator is external and comprises a winding and a yoke. This yoke can be made of a ferromagnetic material or not. The topology of this bearing is very simple and allows to build a device using existing components developed for electrical motors, thereby reducing production costs.

In such a bearing with a radial magnetic field, the material of the winding yoke impacts the bearing performance. The goal of this paper is to investigate about the advantages associated with the presence of a ferromagnetic yoke.

In section II, the bearing topology is presented. In section III, a 2-D analytical model of multipole electrodynamic bearing is summarized. This model gives the forces between the rotor and the stator of the bearing, and the root-loci plot of the centering bearing is derived from it. The way to evaluate the bearing stiffness and stability on the basis of the root-loci plots is exposed in section IV and a comparison is made in section V.

II. Bearing topology

The internal rotor of the proposed bearing comprises a ferromagnetic shaft surrounded by permanent magnets. These magnets induce a radial magnetic field with p pole pairs in the airgap. The external stator of the bearing comprises an airgap axial winding with $q = p+1$ pole pairs, k phases and a yoke. The $p = 1, q = 2$ case with three phases is illustrated in Fig. 1. The geometrical parameters of the bearing are given in Fig. 2. As demonstrated in [7], verifying identity $q = p+1$ ensures that the winding is null-flux and that it can interact with the permanent magnets to produce a radial centering force.

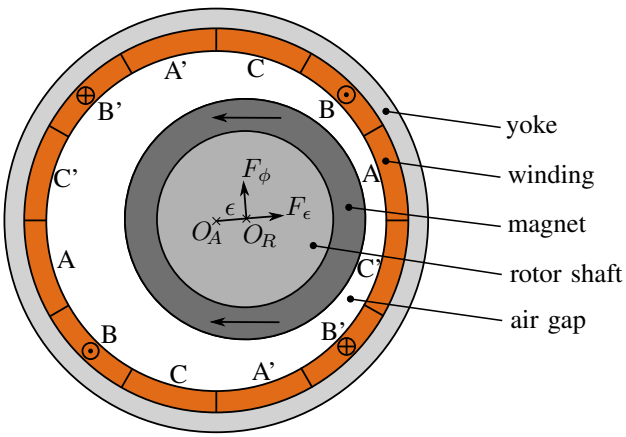

Figure 1. Bearing topology with $p = 1, q = 2$ and $k = 3$. The phases are denoted A, B and C. The airgap width is exaggerated.

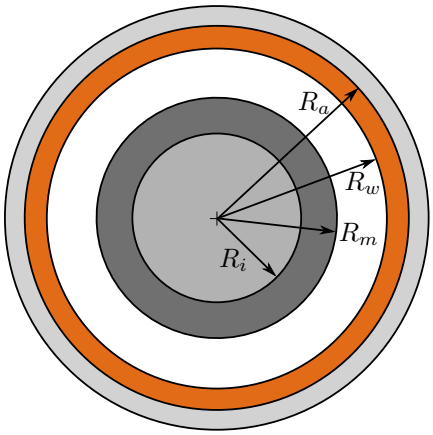

Figure 2. Geometrical parameters of the bearing.

III. Forces

A 2-D analytical model was built to calculate the electromagnetic forces between the rotor permanent magnets and the windings of the bearing when the rotor is off-centered. This model is similar to the one used in [8], and only the main steps are given in this section.

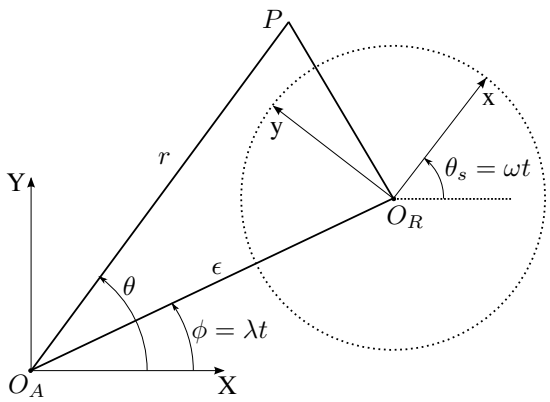

Figure 3. Coordinates of the model.

The coordinates used in this model are shown in Fig. 3. The rotor center is O_R, the armature center is O_A and the axes $x-y$ and $X-Y$ are attached to the rotor and to the stator, respectively. The position of the rotor and the expressions of the magnetic fields are given by coordinates (ϵ, ϕ) and (r, θ), respectively. As illustrated in Fig. 3, the rotor spins around its axis at speed ω and whirls around the axis of the winding at speed λ. To build the model, the following assumptions are made:

1) the end effects are not considered and the problem is assumed to be two-dimensional;
2) the permanent magnets have a linear magnetic characteristic, the rotor shaft is made of a ferromagnetic material with infinite magnetic permeability, and the winding and the permanent magnets have the same magnetic permeability as air. The magnetic permeability of the yoke is either infinite or the same as air, depending on whether the bearing has a ferromagnetic yoke or not;
3) Eddy current losses in the magnets and ferromagnetic parts are neglected;
4) the amplitude of the off-centering ϵ is small compared to the nominal airgap of the bearing;
5) ω and λ are constants and the electrical variables are in a steady-state regime;
6) when calculating the electromotive force in the winding, the effects of the displacement in the radial direction $\frac{d\epsilon}{dt}$ are assumed to be much smaller than ω and λ.

The goal of the model is to obtain the forces between the rotor and the stator of the bearing. These forces are calculated using the Maxwell stress tensor. For this purpose, the magnetic field created by the permanent magnets and by the currents induced in the winding should be calculated. This requires to calculate the induced currents which in turn depend on the electromotive force (emf), the phase resistance and the cyclic inductance of the winding.

First, the analytical expression of the vector potential from the permanent magnets was obtained from [9] and [7]. Because of hypothesis 1 from the previous list, it only has an axial component, and because of hypothesis 3 only the first order terms in ϵ were kept in the Taylor developments of the magnetic vector potential:

$$\begin{aligned} A_{Mz}(r,\theta) = \sum_{n,odd}^{\infty} \Big\{ & C_n(r)\sin\left(np(\theta-\theta_s)\right) \\ & + \epsilon\hat{C}_n(r)\sin\left((np+1)\,\theta - np\theta_s - \phi\right) \\ & + \epsilon\check{C}_n(r)\sin\left((np-1)\,\theta - np\theta_s + \phi\right) \Big\} \end{aligned} \tag{1}$$

with:

$$\begin{aligned} C_n(r) &= K_{1n}r^{-np} + K_{2n}r^{np} \\ \hat{C}_n(r) &= K_{1n}r^{-np-1}np + K_{5n}r^{np+1} + K_{6n}r^{-np-1} \\ \check{C}_n(r) &= -K_{2n}r^{np-1}np + K_{3n}r^{np-1} + K_{4n}r^{-np+1} \end{aligned} \tag{2}$$

In (2), coefficients $K_{1n}, ..., K_{6n}$ are constants which depend on the geometry and on the magnetic properties of the rotor permanent magnets. The magnetic field fundamental harmonic has p pole pairs and the higher-order harmonics have np pole pairs with n being an odd number only. When the rotor is centered, $\epsilon = 0$ and only the terms with C_n remain in (1). When the rotor is off-centered, $\epsilon \neq 0$ and other harmonics appear. They correspond to the terms with $\hat{C}_n$ and $\check{C}_n$ in (1) and their amplitudes are proportional to ϵ.

The magnetic flux created by the permanent magnets in the winding phase i is denoted Φ_{Mi} and can be calculated as follows:

$$\Phi_{Mi} = L\int_{R_w}^{R_a}\int_{0}^{2\pi} A_{Mz}(r,\theta)\frac{J_i(r,\theta)}{I_i} r d\theta dr, \tag{3}$$

where L is the axial length of the bearing, and $J_i(r,\theta)$ and I_i are the current density and the current amplitude in phase i, respectively. For phase i in an axial winding with k phases:

$$\begin{aligned} &\frac{J_i(r,\theta)}{I_i} = \frac{2kqN(-1)^v}{\pi|R_a^2 - R_w^2|} \text{ if } r \in [R_w, R_a] \text{ and} \\ &\theta \in \left[\delta_i + \frac{\pi(k-1)}{2kq} + \frac{\pi v}{q}, \delta_i + \frac{\pi(k+1)}{2kq} + \frac{\pi v}{q}\right], \end{aligned} \tag{4}$$

and $\frac{J_i(r,\theta)}{I_i} = 0$ otherwise. In this expression, $\delta_i = \frac{\pi i}{qk}$ is the angular position of phase i and $v \in \{0; 2q-1\}$. The Fourier development of this function is:

$$\frac{J_i(r,\theta)}{I_i} = \sum_{m,odd}^{\infty} \frac{8Nkq}{\pi^2 m|R_a^2 - R_w^2|} \sin\left(\frac{m\pi}{2}\right) \sin\left(\frac{m\pi}{2k}\right) \sin\left(mq\left(\theta - \delta_i\right)\right). \tag{5}$$

Because $q = p + 1$, only the terms with coefficients $\hat{C}_n$ and $\check{C}_n$ in (1) can give a non-zero contribution to Φ_{Mi}, as exposed in [7]. The amplitude of Φ_{Mi} is thus proportional to ϵ too, as well as the corresponding emf induced in a phase i of the winding. Given hypothesis 5, it can be calculated as:

$$\begin{aligned} emf &= -\frac{d\Phi_{Mi}}{dt} = -\frac{\partial \Phi_{Mi}}{\partial \theta_s}\omega - \frac{\partial \Phi_{Mi}}{\partial \phi}\lambda \\ &= \sum_{m,odd}^{\infty} \Big\{ \epsilon \hat{E}_m \sin\left((mq-1)\theta_s - mq\delta_i + \phi\right) \\ &\quad + \epsilon \check{E}_m \sin\left((mq+1)\theta_s - mq\delta_i - \phi\right) \Big\}. \end{aligned} \tag{6}$$

In this expression, $\hat{E}_m$ and $\check{E}_m$ are constants depending on the geometry and magnetic properties of the winding, as well as the operating speed and pole pair numbers of the rotor and winding. These constants may cancel for some m.

To illustrate this, let us consider the first vector potential harmonic with coefficient $\hat{C}_{n=1}$ in (1). It has $(p+1)$ pole pairs which is the same as the winding. Therefore, it induces a non-zero time-varying magnetic flux in the winding and $\hat{E}_1 \neq 0$.

Let us continue with the model. Knowing the induced emf_i from (6) allows to calculate the current I_i in phase i through:

$$\begin{aligned} I_i = \sum_{m,odd}^{\infty} \Bigg\{ & \epsilon \hat{E}_m \frac{\sin\left((mq-1)\theta_s - mq\delta_i + \phi - \hat{\varphi}_m\right)}{\sqrt{R^2 + ((mq-1)\omega + \lambda)^2 L_c^2}} \\ & + \epsilon \check{E}_m \frac{\sin\left((mq+1)\theta_s - mq\delta_i - \phi - \check{\varphi}_m\right)}{\sqrt{R^2 + ((mq+1)\omega + \lambda)^2 L_c^2}} \Bigg\} \end{aligned} \tag{7}$$

with:

$$\hat{\varphi}_m = atan\left(\frac{((mq-1)\omega + \lambda)L_c}{R}\right)$$
$$\check{\varphi}_m = atan\left(\frac{((mq+1)\omega + \lambda)L_c}{R}\right)$$

where R and L_c are the winding phase resistance and cyclic inductance, respectively. The phase difference between emf_i and I_i is denoted φ_m. The previous reasoning can be repeated for every winding phase. Once the current in each phase is known, the magnetic field created by this current in the airgap is found by solving Maxwell's equation for the magnetic field in the airgap. This was done in [10] for the bearing with a ferromagnetic yoke and a similar approach was used in the yokeless case. The magnetic field B_I in the airgap due to the induced current flowing in the entire winding is obtained by summing the contributions of each phase. Because of hypothesis 2 at the beginning of this section, the total magnetic field B_{tot} in the airgap is the sum of the magnetic field from the winding and from the rotor permanent magnets:

$$\vec{B}_{tot} = \vec{B}_M + \vec{B}_I, \tag{8}$$

with $\vec{B}_M = \nabla \times \vec{A}_{Mz}$. Finally, the force between the rotor and the winding was obtained by integrating Maxwell's stress tensor in the airgap. This allows to obtain the force component acting on the rotor in the direction of the off-centering and in the direction perpendicular to it F_ϵ and F_ϕ, see Fig. 1:

$$\begin{aligned} F_\epsilon &= \int_0^{2\pi} \left\{ \frac{1}{2\mu_0}\left(B_{tot,r}^2 - B_{tot,\theta}^2\right)\cos(\theta - \phi) - \frac{B_{tot,r}B_{tot,\theta}}{\mu_0}\sin(\theta - \phi) \right\} Lrd\theta; \\ F_\phi &= \int_0^{2\pi} \left\{ \frac{1}{2\mu_0}\left(B_{tot,r}^2 - B_{tot,\theta}^2\right)\sin(\theta - \phi) + \frac{B_{tot,r}B_{tot,\theta}}{\mu_0}\cos(\theta - \phi) \right\} Lrd\theta; \end{aligned} \tag{9}$$

where $B_{tot,r}$ and $B_{tot,\theta}$ are the radial and azimuthal components of the magnetic field, respectively. As will be shown in the next sections, these forces may be pulsating. The time averages of these forces are obtained by removing the time-dependent terms in (9) and are denoted $\bar{F}_\epsilon$ and $\bar{F}_\phi$. In the next sections, the pulsating component is neglected compared to the time average forces on the bearing rotor. Indeed, pulsating forces can be reduced by increasing the number of phases [7].

IV. Performance evaluation

In this section, the effects of $\bar{F}_\epsilon$ and $\bar{F}_\phi$ on the stability of the bearing is first exposed. Then, a way to compare two bearings with and without ferromagnetic yoke using the model developed in the previous section is presented.

Due to the assumptions exposed in section II, the forces predicted by the model are directly proportional to ϵ. Therefore, the effects of $\bar{F}_\epsilon$ and $\bar{F}_\phi$ can be associated with stiffnesses K_ϵ and K_ϕ through $\bar{F}_\epsilon = -K_\epsilon\epsilon$ and $\bar{F}_\phi = -K_\phi\epsilon$.

When $K_\epsilon > 0$, it has a positive effect since it is acting on the rotor toward the axis of the winding, see Fig. 1. On the contrary, K_ϕ has a negative effect on the stability of the bearing whatever its sign. It induces a whirling motion of the rotor around the axis of the winding, resulting in centrifugal forces acting on the rotor. These centrifugal forces grow and finally overcome K_ϵ, thereby preventing the rotor from coming back toward the center of the winding. Finally, it appears that such a bearing is not stable without providing additional damping to cancel the effect of K_ϕ. This is consistent with [5], [11], [12] and with the results from the next sections. Since it is widely acknowledged that adding contactless damping in the system by passive means is not easy, the amplitude of $\bar{F}_\phi$ should therefore be minimized.

In order to compare or optimize electrodynamic bearings, it is necessary to evaluate their performance objectively. For this purpose, looking at $\bar{F}_\epsilon$ and $\bar{F}_\phi$ is not sufficient since it does not give the amount of damping which must be added to have a stable bearing e.g..

Let us show how a root loci plot can be used to evaluate the performance of a bearing objectively. This has been used in previous works on the stability of a system comprising electrodynamic bearings. In [13], a parametric model was derived. It was validated by identification of the parameters with experimental data and by showing that the predicted stability threshold spin speed corresponds with experimental results. Compared with the model exposed in the previous section, the model from [13] can be used with homopolar and heteropolar bearings and neither requires to derive the current amplitude nor to make assumptions 1, 5 and 6 from the previous section. However, this model alone cannot be used in a design optimization process because the parameters depend on the bearing geometry and must be identified first.

Let us derive the root loci plot using the 2-D model exposed previously. Using complex numbers for vector quantities and noting the position of the rotor $z = X + jY = \epsilon e^{j\phi}$, the motion equation of the rotor is:

$$m\ddot{z} + c\dot{z} + K_\epsilon z + jK_\phi z = 0, \tag{10}$$

where $j = \sqrt{-1}$, m is the rotor mass and c is the external damping added in the system. The stiffnesses K_ϵ and K_ϕ are calculated for a fixed spin speed ω and a zero whirl speed λ because $\lambda << \omega$. This will be validated later in this section. The governing set of equations of the associated state-space model are:

$$\begin{bmatrix} \ddot{z} \\ \dot{z} \end{bmatrix} = \mathbf{A} \begin{bmatrix} \dot{z} \\ z \end{bmatrix} + \frac{1}{m}\mathbf{B}, \tag{11}$$

with:

$$\mathbf{A} = \begin{bmatrix} \frac{-c}{m} & \frac{-K_\epsilon - jK_\phi}{m} \\ 1 & 0 \end{bmatrix}. \tag{12}$$

In (11), matrix $\mathbf{B}$ is the external input force matrix and $\mathbf{A}$ is the dynamic matrix whose eigenvalues give the root loci plot. The two eigenvalues are:

$$\rho_{1,2} = \frac{-c}{2m} \pm \sqrt{\left(\frac{c}{2m}\right)^2 - \frac{K_\epsilon + jK_\phi}{m}}. \tag{13}$$

The root loci of a system comprising a bearing without additional damping is shown in Fig. 4 for different speeds ω and yoke material. This was obtained for a bearing with the dimensions from Table I and with a rotor mass $m = 50[kg]$. The permanent magnet at the rotor has a parallel magnetization pattern with $p = 1$ and a remanent magnetic field density $B_{rem} = 1.32[T]$. The winding has two pole pairs and three phases.

Table I
BEARING DIMENSIONS $[mm]$.

R_i	R_m	R_w	R_a	L
2	18	19	21	70

As can be seen in Fig. 4, there is a rotational symmetry with respect to the origin so that whatever the material of the yoke, one of the two roots of the system is always on the right-hand side of the plane i.e., its real part is positive. This indicates that

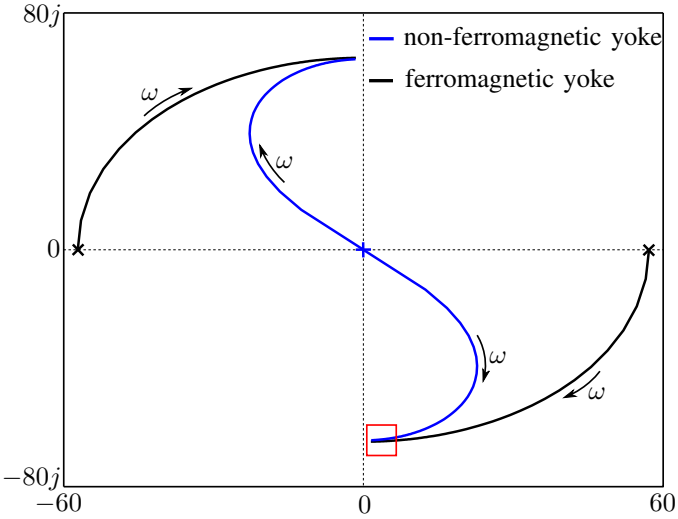

Figure 4. Root loci for $\omega \in [0, 2\pi 5000]$ and $c = 0$. The arrows show the direction of increasing ω.

the bearing is always unstable when no damping is added in the system and it corresponds to expectations. As ω increases, the winding becomes more inductive, F_ϵ (and K_ϵ) reach a maximum value while F_ϕ (and K_ϕ) decrease toward zero. The unstable root approaches the stability region on the left-hand side of the plane and $|\Re\{\rho\}| << |\Im\{\rho\}|$, see the region with a red square in Fig. 4. Let us focus on the behaviour of the unstable roots in this region. The root-loci is drawn for $c = 0$, so in this case (13) becomes:

$$\rho_{1,2} = \pm j\sqrt{\frac{K_\epsilon + jK_\phi}{m}}. \tag{14}$$

If the unstable root of the root loci with $c = 0$ is such that $|\Re\{\rho\}| << |\Im\{\rho\}|$, two observations can be made. Firstly, $K_\phi << K_\epsilon$ and therefore $\Im\{\rho_{1,2}\}$ can be associated with the stiffness K_ϵ toward the center of the stator through:

$$\Im\{\rho_{1,2}\} \approx \pm\sqrt{\frac{K_\epsilon}{m}}. \tag{15}$$

Secondly, if a reasonable amount of damping c is introduced to make the unstable root reach the imaginary axis toward the stability region, it can be derived from (13) that $\Re\{\rho\}$ moves $-\frac{c}{2m}$ to the left.

From these two observations, it appears that the stability and the stiffness of a bearing can be evaluated separately. Therefore, if two bearings with a same mass m and damping $c = 0$ are operating in a region such that $|\Re\{\rho\}| << |\Im\{\rho\}|$, looking at their real and imaginary parts allows to know which one has the greatest stiffness and/or needs less damping to be stable.

The assumption $\lambda << \omega$ can be validated as follows. When no external damping is added to the bearing, it was observed that the rotor trajectory is an outward spiral and that the value of λ quickly reaches a constant value given by $|\Im\{\rho\}|$. The evolution of this value with ω is given in Fig. 5, showing that the assumption $\lambda << \omega$ is valid whatever the value of ω.

Finally, let us add that these results are limited to bearings operating in a region such that $|\Re\{\rho\}| << |\Im\{\rho\}|$. However,

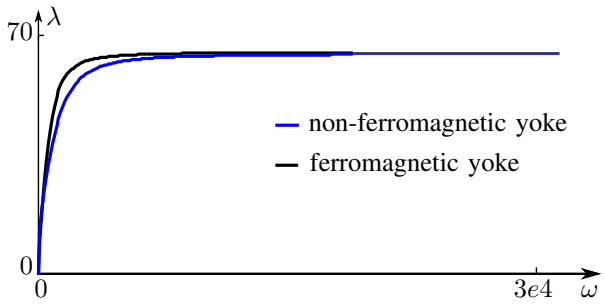

Figure 5. Evolution of the whirl speed λ with ω.

this assumption is not very constraining as this is the operating region that will be preferred when considering the difficulty of adding external damping in the system.

V. Bearing comparison

Using the results from the previous section, let us show an example of comparison between two bearings with and without ferromagnetic yoke. The study is based on the following assumptions. Both bearings have the same rotor and the same air gap thickness. Therefore, the bearings' rotors have the same mass m and the only remaining geometrical variable is R_a, see Fig. 2. The default geometrical and magnetic parameters are the same as in the previous section.

The selection process for the best bearing is the following. The bearings have to provide a minimum stiffness when operating above a given threshold speed. The best bearing will be the one meeting these requirements and requiring the less damping to reach stability.

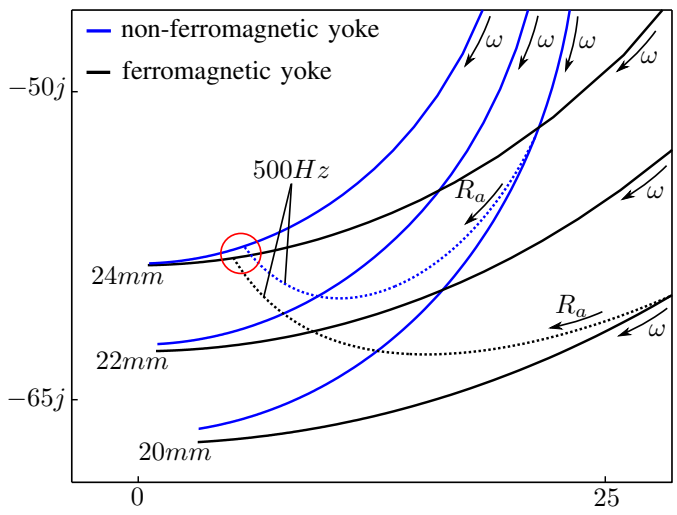

Figure 6. Unstable poles in the area of interest of the root loci for $c = 0$. The dotted (solid) lines correspond to a fixed ω (a fixed Ra).

Fig. 6 shows a zoom on the area of interest in the root loci plot. The dotted lines were obtained for a fixed speed ω and an increasing radius R_a. They give the minimum operating speed of the two bearings so that the area of interest with $\omega > 2\pi 500$ is below these curves. The solid lines were obtained for the fixed radii $R_a = 20, 22, 24[mm]$ and an increasing speed ω. The evolution of the bearing properties with speed can thus be observed by following these solid lines in the region above the threshold speed. The performance of a bearing for a given set of parameters (R_a, ω) is obtained by looking at the crossing points between the corresponding dotted and solid lines. E.g., two such points for $(R_a = 24[mm], \omega = 500[Hz])$ are in the red circle of Fig. 6. For this set of parameters, the bearing with a ferromagnetic yoke has a better stiffness and better stability properties. Looking at Fig. 6, it is clear that the bearing performance improve with speed.

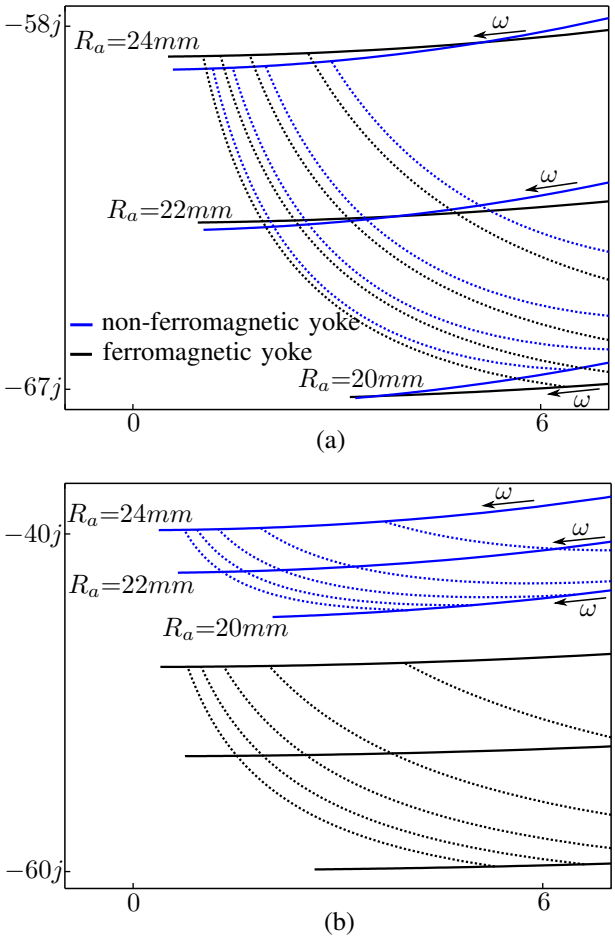

Figure 7. Root loci of the bearings with no damping, $p = 1$ and $R_i = 0[mm]$ (a) or $R_i = 10[mm]$ (b).

In order to see the evolution of the previous result with ω and R_a, more data is needed, as shown in Fig. 7. This was obtained for different rotor shaft radii $R_i = 0[mm]$ and $10[mm]$. From Fig. 7 (a), it appears that the yoke material does not have a significant influence on the bearing stiffness and stability in the area of interest when $R_i = 0[mm]$. E.g. for $R_a = 24[mm]$, a bearing with a ferromagnetic yoke has a better stiffness but is less stable than a bearing with no ferromagnetic yoke, but the differences are not very significant. However, these differences increase with R_i as shown in Fig. 7 (b). Comparing the corresponding points

for each kind of yoke, it appears that the bearing with a ferromagnetic yoke has a significantly greater stiffness but is less stable. Finally, the stiffness of the two kinds of bearing decrease with R_i, which is consistent with intuition since the amount of permanent magnet decreases with R_i.

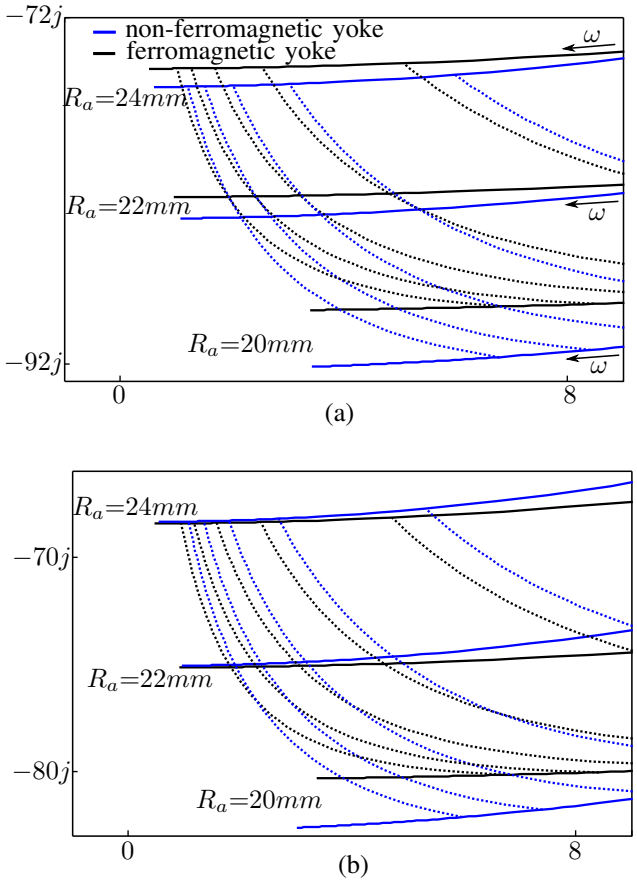

Figure 8. Root loci of the bearing without damping, $p = 2$ and with $R_i = 0[mm]$ (a) or $R_i = 10[mm]$ (b).

Fig. 8 shows the same data than Fig. 7, except that the pole pairs number of the rotor and of the winding are $p = 2$ and $q = 3$. The permanent magnets still have a parallel magnetization pattern. Looking at Fig. 8 (a), it appears that the stiffnesses of the bearings are improved but the differences between the bearings with and without ferromagnetic yoke remain small and the situation is similar to Fig. 7 (a). Fig. 8 (b) shows that increasing the shaft radius R_i is less favourable for the bearing without ferromagnetic yoke, but the difference between Fig. 8 (a) and (b) is much smaller than the difference between Fig. 7 (a) and (b). Last but not least, the bearing with a ferromagnetic yoke has a lower stiffness the the bearing without ferromagnetic yoke when $R_i = 20[mm]$ i.e., when the yoke is close to the permanent magnets. This is due to the higher order harmonics in the permanent magnet field. They contribute to the negative stiffness associated with the reluctant force between the permanent magnets and the ferromagnetic yoke, but they do not contribute to the centering Lorentz force between the permanent magnet and the winding. This effect cancels as R_a increases and was not observed with $p = 1$ because there was no higher order harmonics in the permanent magnet field in this case.

VI. Conclusion

In this paper, the influence of the magnetic permeability of the yoke on the behaviour of electrodynamic bearings was studied. To this end, a 2-D analytical model was presented and used to draw the root loci plot of the bearings without external damping. Considering the difficulty of adding the external damping to the bearing which is necessary to achieve stability, the area of interest to operate an electrodynamic bearing was identified in the root loci plot. Then, a way to use this plot to evaluate the stiffness and stability properties of the bearings independently was presented. Finally, this model was used to compare bearings with and without a ferromagnetic yoke.

It was shown that the yoke material does not have a significant influence on the performance of the bearing for a small rotor shaft radius. As this radius increases, the stiffness of the bearing decreases and this effect is more significant for a bearing without ferromagnetic yoke. Also, increasing the pole pairs number of the bearing has a positive effect on the bearing stiffness but is less advantageous for a bearing with a ferromagnetic yoke when the yoke is close to the permanent magnets. Finally, this paper shows that choosing the yoke material is not a trivial issue and requires a more comprehensive optimization process to be carried out.

References

[1] G. Schweitzer and E. H. Maslen, "Magnetic bearings: theory, design and application to rotating machinery," *Springer*, 2009.

[2] A. Looser and J. Kolar, "An active magnetic damper concept for stabilization of gas bearings in high-speed permanent-magnet machines," *IEEE Trans. Ind. Electron., vol.61, No 6*, pp. 3089–3098, 2014.

[3] R. F. Post and D. D. Ryutov, "Ambient-temperature passive magnetic bearings: Theory and design equations," *Proceedings of the Sixth International Symposium on Magnetic Bearings*, 1998.

[4] R. F. Post and D. A. Bender, "Ambient-temperature passive magnetic bearings for flywheel energy storage systems," *Proceedings of the Seventh International Symposium on Magnetic Bearings*, 2000.

[5] A. V. Filatov and E. H. Maslen, "Passive magnetic bearing for flywheel energy storage systems," *IEEE Trans. Magn., vol.37, No 6*, pp. 3913–3924, 2001.

[6] T. A. Lembke, "Design and analysis of a novel low loss homopolar electrodynamic bearing," *Ph.D. dissertation, Royal Inst. Tech., Sweden*, 2005.

[7] C. Dumont, V. Kluyskens, and B. Dehez, "Null flux radial electrodynamic bearing," *accepted for publication*.

[8] C. Dumont, V. Kluyskens, and B.Dehez, "Yokeless radial electrodynamic bearing," *11th International Conference on Modeling and Simulation of Electric Machines, Converters and Systems 'Electrimacs'*, 2014.

[9] A. Rahideh and T. Korakianitis, "Analytical open-circuit magnetic field distribution of slotless brushless permanent-magnet machines with rotor eccentricity," *IEEE Trans. Magn., vol.47, No 12*, pp. 4791–4808, 2011.

[10] K. Atallah, Z. Zhu, D. Howe, and T. Birch, "Armature reaction field and winding inductances of slotless permanent-magnet brushless machines," *IEEE Trans. Magn, vol.34, No 5*, pp. 3737–3744, 1998.

[11] V. Kluyskens and B. Dehez, "Dynamical electromechanical model for magnetic bearings subject to eddy currents," *IEEE Trans. Magn., vol.49, No 4*, pp. 1444–1452, 2013.

[12] A. Tonoli, N. Amati, F. Impinna, and J. G. Detoni, "A solution for the stabilization of electrodynamic bearings: Modeling and experimental validation," *J. Vib. Acoust., vol.133, No 2*, 2011.

[13] J. Detoni, F. Impinna, A. Tonoli, and N. Amati, "Unified modelling of passive homopolar and heteropolar electrodynamic bearings," *J. Sound Vibration, vol.331, No 19*, pp. 4219–4232, 2012.